CFD AND PIV BASED INVESTIGATION OF INDOOR AIR FLOWS DOMINATED BY BUOYANCY EFFECTS GENERATED BY HUMAN OCCUPANCY AND EQUIPMENT

Rehan Yousaf[1], Daniel Wood[2], Malcolm Cook[1],Tong Yang[1], Simon Hodder[1], Dennis Loveday[1] and Martin Passmore[2]

[1] Department of Civil & Building Engineering, Loughborough University, UK
[2]Department of Aeronautical and Automotive Engineering, Loughborough University, UK

ABSTRACT

This paper describes the full scale tests for air flows in a test chamber subject to heat loads generated by human occupancy and equipment. The Particle Image Velocimetry (PIV) technique was used to investigate buoyancy-driven flows near the human thermal manikin "Victoria". Based on the experimental facility details, a full scale 3-D CFD model of the test facility was generated. The results obtained from the CFD simulation were compared with data obtained from the PIV results. Results compare very well and demonstrate the potential usefulness of PIV as a CFD validation technique.

INTRODUCTION

Natural convection effects due to human metabolic heat give rise to air flow around the human body. This flow influences the movement of bio effluents and heat transfer mechanisms around the body.

This thermally generated natural convective flow has a direct influence on the Indoor Air Quality (IAQ) and indirectly on the complete heating ventilation and air conditioning (HVAC) system. The importance of this thermally induced flow due to human metabolic heat has led to many investigations on this subject. A number of studies have reported the buoyancy driven flow generated due to the metabolic heat release of the human body. The measure of this buoyancy driven flow is the air velocity above the head region. The magnitude of this air velocity influence the phenomena such as entrainment and entrapment of surrounding air and contaminants.

Homma and Yakiyama (1998) in their experiments used infrared thermograms for observing temperature distribution around subjects along with smoke wire photography and hot wire anemometers to measure local velocities. Their results show that the velocities above the head range between a minimum of 0.05 m/s to a maximum of 0.3 m/s for standing subjects.

Another experimental study by Clark (1974) reported velocities exceeding 0.3 m/s above the head region. Borges et al (2002) and Sideroff (2005) in their validation experiments reported maximum velocity of between 0.3 m/s and 0.4 m/s at 40 cm above the head. Özcan and his colleagues (2005) investigated flow surrounding the human head and reported a maximum vertical air velocity of about 0.38 m/s. Recent experimental work from Spitzer (2010) based on PIV measurements reported air velocities of about 0.3 m/s near the head region.

With the development in numerical techniques and computational resources in the past 10 years, a number of researchers modelled the buoyancy induced flows using Computational Fluid Dynamics. In CFD, Computer Simulated Persons (CSPs) or Computer Thermal Manikins (CTMs) with different level of details are modelled. Cropper et al. (2008) and Yang et al. (2007) simulated standing postures with buoyancy dominated flows. The maximum velocity reported in the thermal plume was 0.4 m/s.

Sorensen et al. (2003) simulated seated subjects and reported maximum velocities between 0.4 and 0.5 m/s. A number of other researcher such as Murakami et al. (1997), Topp et al C (2002), Hayashi.et al. (2002) carried out CFD simulations and reported maximum air flow velocities for seated CTMs between 0.17 m/s and 0.26 m/s.

Based on previous simulation and experimental work, it is seen that the maximum air velocities generated due to thermal buoyancy effects above and around the human body vary between 0.17 m/s to 0.5 m/s. The experimental work that has been carried out so far has used different measuring techniques ranging from simple hot wire anemometer and smoke tracing to highly sophisticated Particle Image Velocimetery (PIV) and Phase Doppler Anemometry (PDA).

As the temperature and velocity values measured in buoyancy induced flows above humans are very small, any intrusive measuring techniques can lead to inaccuracy in results. Non intrusive techniques such as PIV and PDA are preferable, but are expensive both in terms of time and money. On the other hand, CFD simulations require advanced knowledge about correctly modelling the physical phenomena such as turbulence, heat and mass transfer etc.

Much effort is being put in the experimental validation of CFD models using both intrusive and non-intrusive measuring techniques. The validation work on one side helps recognize the limitations and hurdles associated with experimental techniques and on the other helps improve the numerical models.

The work presented in this paper is one such effort to validate the buoyancy induced flow predicted by a CFD simulation of a female seated non-breathing thermal manikin "Victoria" using PIV techniques.

EXPERIMENTAL SETUP

The experimental chamber has the dimensions of 5.43×3.09×2.4 m in length, width and height, as shown in Figure 1 below. Three thermocouples were attached to the internal surface of each side wall giving wall surface temperature. In addition to the thermocouples 4 hobo data loggers (HT1, HT2, HT3 and HT4) were suspended to give air temperature at defined points. A thermocouple (TC1) was suspended above Victoria in order to capture the plume temperature. TC1 had to be adjusted to avoid the line of laser sheet (in order to avoid any reflection problems). The co-ordinates of these points are given with respect to the surrounding walls in Table. 1 and are shown graphically in Figure 2. The thermal manikin Victoria was kept at a constant surface temperature of 34° C.

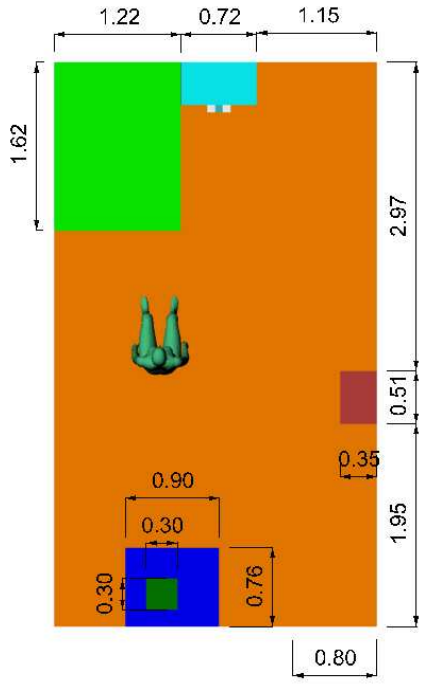

Figure 1 Dimensions of the experimental chamber in metres.

In order to capture the flow field, a LaVision GmbH (LaVision, 2011) PIV system was utilised for the current experimental work, consisting of two 4MP (2048x2048 pixel) cameras, a dual cavity 200mJ/pulse Nd:YAG laser, a 4 nozzle Laskin type seeder and associated timing, processing and calibration equipment.

The location of the equipment is shown in Figure 3 with the laser mounted in front of the manikin and the cameras mounted perpendicularly to the sheet ~1.5m to the manikin's LHS. Due to issues with reflections at the laser sheet/manikin head intersection the sheet was positioned ~1x10-3 m behind the centreline, shielding the reflections with the natural curvature of the manikins head.

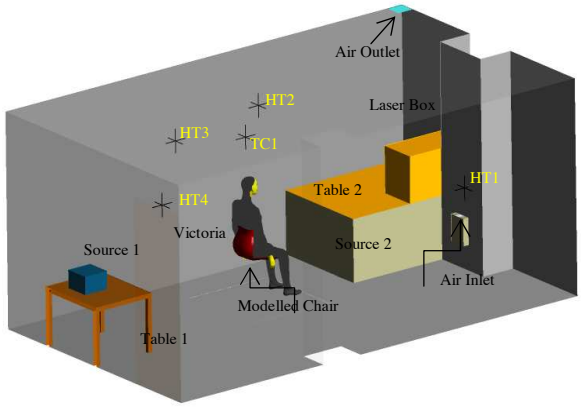

Figure 2 Visualization of test chamber with location of different sensors.

Table. 1

Co-ordinates of the installed sensors in test chamber.

SENSOR NAME	DISTANCE FROM WALL [m]		
	LEFT	FRONT	ABOVE FLOOR
HT1	1.67	0.45	0.91
HT2	2.66	5.33	2.04
HT3	0.88	3.78	1.94
HT4	1.13	2.83	2.19
TC1	1.02	2.93	1.84

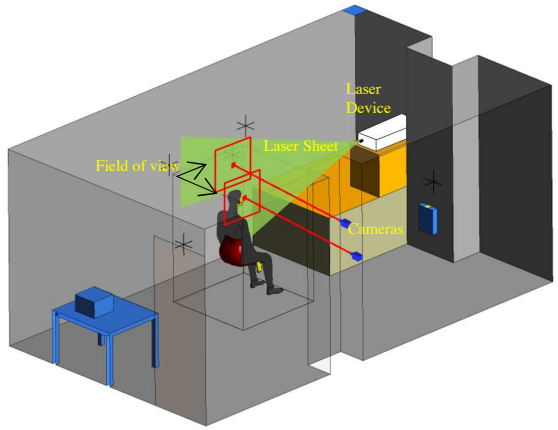

Figure 3 Visualization of test chamber with setup of PIV apparatus.

The body of the thermal manikin was covered with black skin- tight clothing to minimize reflections from the body. The wall behind the manikin was also covered with a black covering for reflection reasons. A raw image showing the combined, ~1.0x0.5m, FoVs from both cameras is presented in Figure 4. The lower camera was positioned in such a way that the manikin's head was located toward the rear of the FoV, reducing the area of the frame in the laser shadow. The upper camera was located so the FoV was centred about the manikins head to centre the

thermal plume within the frame. During the calibration procedure, a calibration plate was positioned to be visible in both frames with a row of markers present in the frame overlap; thereby ensuring the frames relative location and rotation could be accurately determined. Seeding was performed using a 4 nozzle Laskin type seeder placed in the centre of the experimental chamber. This device produced seeding particle with a diameter of ~1x10^{-6} m, using olive oil. This was selected for its large refractive index, making particles highly

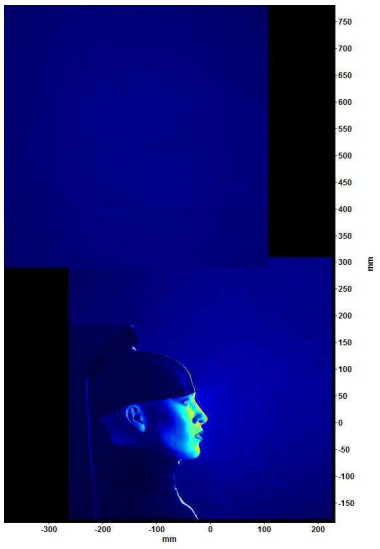

Figure 4 Raw PIV camera images showing the two FoVs´, one above the other.

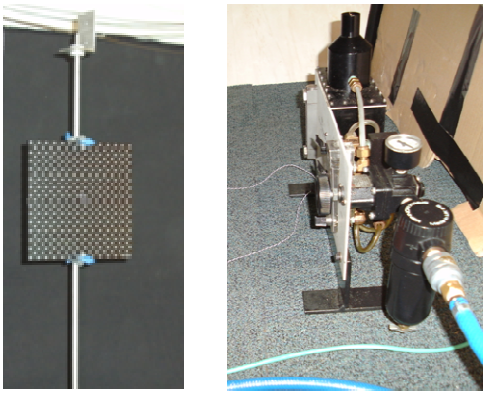

Figure 5 Photograph of the calibration plate (left) and seeder (right) used in the experiments.

visible, being close to neutrally buoyant, sinking at ~1x10-10 m/s assuming Stokes flow and having extremely fast particle response time, O1x10-9s, allowing the clear resolution of highly turbulent structures. The calibration plate and seeder device are shown in

Figure *5*.

SIMULATION METHODOLOGY

3-D Model and Mesh Generation

The CSP model is a female manikin manufactured by PT.Teknik, Denmark. The geometrical model for CFD calculations has been used in a number of previous studies used for investigation of indoor human thermal comfort, air pollution and respiration (Melikov et al., 1998, Tanabe et al., 1994, Melikov et al., 2002). The 3-D scanned data of the thermal manikin "Victoria" was taken from the work published by Nielsen et al. (2003). The model was refined using the 3-D modelling software Rhinoceros version 4 (Robert McNeel & Associates 2010).

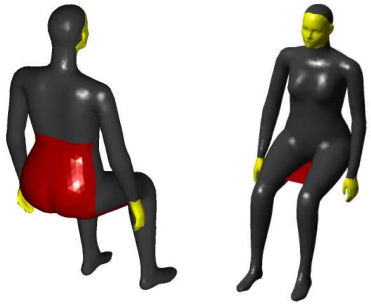

Figure 6 Seated model of thermal manikin "Victoria" with chair (shown in red)

A chair was modelled as a 2-D adiabatic object perfectly in contact with Victoria´s surface to take into account the blockage in airflow as shown in Figure 6.

Using the dimensions of the experimental chamber, a 3-D geometry was prepared in Rhinoceros version 4. Both the geometries i.e. the geometry of the thermal manikin and that of the test chamber were merged in a single model. The region around the seated Victoria was further enclosed in a virtual box dimensioning 1.1m * 1.1 m * 1.6 m. This virtual box denotes an inner fluid domain and serves two major purposes i.e. a) provide a better mesh control by refining the region of interest b) provide a confined space to evaluate thermal comfort which can be very useful when investigating multiple instance cases.

As the geometrical model was divided into two regions, the meshing was carried out using ANSYS ICEM CFD (Ansys Inc. 2010) for the two zones, namely "virtual comfort domain" with the seated Victoria and "Lab domain" with the rest of the surrounding. In a previous benchmark study for seated thermal manikin in natural convection environment from the author (Yousaf, 2010), the same technique of division between comfort and surrounding zone was used. As the major focus lays in the flow around the manikin (comfort zone), the results of the previous study were used as meshing guidelines for mesh independent results thereby giving approx. 3M volume cells as an optimum mesh size of comfort domain with 9 prism layers on the surface of thermal manikin. The surroundings were modelled with a total volume cells of approx. 1.7 M.

The mesh of the complete model and close up of the meshed thermal manikin is shown in Figure 7. The advantage of following this meshing methodology lies in the efficiency in mesh generation and mesh consistency in regions of interest. Parametric and multiple instance studies can be carried out by merging the virtual comfort zone into almost any surrounding.

A mesh independency check was carried out with the Virtual Comfort Domain (VCD) meshed using different mesh sizes but keeping the maximum surrounding size to 1.7M cells. The detail of the mesh sizes is shown in Table. 2.

Table. 2

Mesh sizes used in Mesh Independency Tests.

NR.	VCD [M]	TEMPERATURE AT TC1 [°C]	Simulation status
1	0.6	22.0	Not converged
2	1.5	22.5	Converged
3	3.0	23.4	Converged
4	5.0	23.3	Converged

The boundary layer around the CSP was kept to be 9 cells in all cases. Only the RNG k-ε turbulence model was used in the mesh independency studies. The sensor point TC1 modelled in the CFD simulations was considered as the judgment criteria for declaring a mesh independent solution. The comparison shows that the temperature difference between cases 3 and 4 at the chosen point is very small. Minor variations in results are observed in regions away from the CSP when plotted for velocity, thereby proving that even with very fine meshes a 1 to 1 similarity is not possible. Due to low computational costs with almost the same level of accuracy when compared to mesh 4, the results obtained using mesh 3 were considered to be mesh independent and the mesh is used for further investigations.

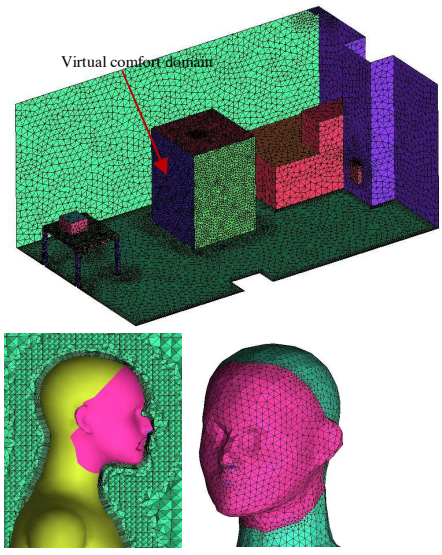

Figure 7 Meshed model of the test chamber along with the virtual comfort domain and detailed meshing of CSP Victoria.

Simulation Parameters

Steady state simulations using the Ideal Gas Law approach were carried out. The discrete transfer surface to surface model was used to model the radiative heat transfer (Siegel, 1993). Solving steady state in ANSYS CFX often requires the use of false time stepping to control convergence (Ansys Inc. 2010). For the current study the flow field is solved using "Local time stepping" methodology which uses different pseudo time steps in different regions of flow. In order to get a faster convergence, the local time steps were multiplied with "time step factor" of 5 for momentum and energy.

Simulations were carried out using SST Turbulence model and RNG-k-e models (Ansys Inc. 2010) using the same mesh. The results obtained were compared against the temperature and flow field (PIV) measurements. Both simulations used a "High Resolution" discretization scheme for advection terms and first order upwind for turbulence quantities as recommended by ANSYS (Ansys Inc. 2010). A "High Resolution" (Ansys Inc. 2010) discretization scheme was employed due to its use of local blending factor between 1st and 2nd order thereby providing an excellent compromise between accuracy and robustness. In order to increase the accuracy of the results, the double precision capability of the unstructured Multigrid ANSYS CFX solver (Ansys Inc. 2010) was used.

In order to account for the viscous forces and the rapid change in variable gradients at and near the wall surfaces, scalable wall function (Ansys Inc. 2010) were used for RNG-k-ε thereby allowing the use of a logrithmic wall function approximation in cases where the mesh was not fine enough near the wall surface for RNG-k-ε Model. For the SST turbulence model the near wall region was resolved using a so called "automatic wall function" (Ansys Inc. 2010) which switches from low Reynolds wall formulation to normal wall functions thereby allowing the use of k-ω model near the wall (where flow dominated by low Reynolds numbers occurs) and k-ε away from the immediate vicinity of wall.

Root Mean Square (RMS) residuals below 1e-5 for mass, momentum and energy were set as convergence criteria. The author´s previous study (Yousaf, 2010) has shown that buoyancy driven flows are often dominated by turbulent structures at different scales and are often difficult to capture using RANS (Reynolds Averaged Navier Stokes) type turbulence models. Such flows often show oscillatory behaviour in the residuals and require additional numerical measures and monitors to achieve convergence. For this reason, along with the RMS residual check, the flow state in the region of interest was additionally monitored by using 3 monitor points set above the manikin´s head in the thermal plume for recording variations in velocity and temperature. A steady converged state was

interpreted when no noticeable fluctuation at these monitor points was seen. An additional imbalance convergence check was applied on all the transport equations. This convergence check assures that even if flow is locally stable and has reached the defined RMS values, there is no imbalance in the equations for momentum, mass and energy. The value of this imbalance convergence check was set to be 1%.

Boundary Conditions

Based on the measurements taken in the experimental chamber, the thermal manikin was given a constant surface temperature of 32.8°C on the clothed region and 34°C on the naked skin parts (face, neck and hands). The inlet was a 7cm × 7cm opening with an inlet air temperature of 19°C and an average flow velocity of 1 m/s. The outlet was modelled as a pressure opening with a relative pressure of 0 Pascal. The surfaces floor, table 1, table 2 and laser box as shown in Figure 2 are modelled as adiabatic surfaces.

For the rest of the surroundings, the boundary conditions are given in the Table. 3 below. (Surface are named per orientations with respect to the thermal manikin i.e. a wall located to the left hand side of Victoria is named as "Left Wall"). All the walls are considered as smooth walls. The wall temperatures are the average temperatures measured using thermocouples attached at various points on the internal wall surface. In addition to the thermocouples, thermal images using a thermal camera were taken at the beginning and end of each experiment and were taken into consideration by averaging the boundary temperatures.

Table. 3

Co-ordinates of the installed sensors in the test chamber.

BOUNDARY NAME	TEMPERATURE [°C]
Right Wall	20.9
Left Wall	21.3
Back Wall	22
Front Wall	22
Ceiling	23
Door	23.2
Source 1	25
Source 2	25

Computational details

All the calculations were carried out on an intel-Xenon 64 cluster using 24, 2.66 GHz processors. The required wall clock time for the calculated cases with 2000 iterations per case was approximately 5 hours.

RESULTS

In order to declare CFD results converged, the convergence criteria mentioned in previous section were checked. Instead of decreasing, the RMS residual values tended to remain static around 1e-2. The reasons were investigated by a) mesh improvement b) plotting regions of high residuals for momentum, mass and energy c) running the same case for 1 minute in transient mode. Mesh improvement had little effect on reducing the residuals. High residuals were found to be near the chair region denoting strong wake and shear regions. The points of maximum residuals are shown by red cross points in Figure 8.

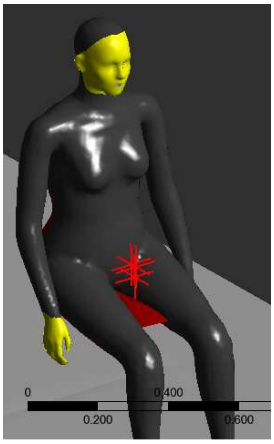

Figure 8 Points of maximum residuals located near to the chair region shown as red cross points.

In order to confirm this local peak in residuals due to transient wakes, a transient (time step 0.1 second) run of 1 minute with initial boundary condition from the steady state case was conducted. The RMS residuals fell far below 1e-6 within the first few seconds of the run confirming the presence of local turbulent structures. In order to overcome the problem, numerical improvements such as Gradient relaxation factor, Blend relaxation factors and setting variable false time stepping schemes etc were applied thereby reducing the RMS residuals down to 3e-4 and improving the flow stability. The details of these factors are beyond the scope of this validation study and therefore will be discussed in separate publications.

For comparison of the two turbulence models and validation against the experiments, the CFD results are presented as a) temperature values at the sensor points installed in the test chamber and b) a velocity field projected on a plane in the vicinity of the thermal manikin. The plane location is the same as the location of the laser sheet in the experiments.

Temperature

Figure 9 shows a comparison of temperature between the simulated and actual measurements at selected sensor points. The location of the sensor points are given in Table. 1.

As PIV captures transient images at approx. 3 Hz, the images were averaged. A typical transient image taken by the PIV measuring technique is shown in Figure 10. The scale is set from 0 m/s to 0.24 m/s. The white zones in the centre denotes values exceeding 0.24 m/s.

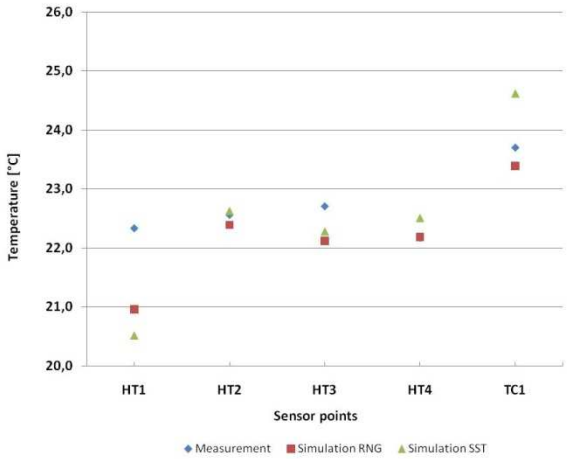

Figure 9 Comparisons of temperatures at the installed sensor points.

Figure 11 is the representation of average velocities projected onto a plane passing through the thermal manikin using PIV.

Figure 12 represent the velocity flow field as a result of CFD simulation using RNG-k-ε Turbulence model on the plane located at dimensional co-ordinates same as those in PIV tests.

Figure 13 represent the velocity flow field as a result of CFD simulation using SST Turbulence model on the plane located at dimensional co-ordinates similar to those in PIV tests.

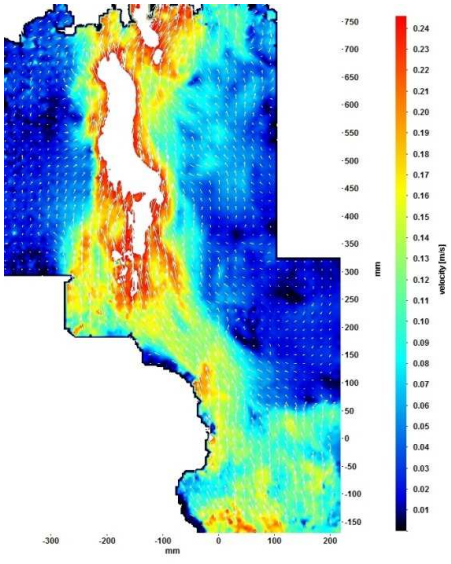

Figure 10 Instantaneous velocity contours obtained using PIV tests in the chamber.

The comparison of temperatures at different sensors placed in the test chamber with the simulation results presented in figure 10 show that CFD simulations represent the test case quite closely taking into consideration that the temperature sensors used in the test chamber have an accuracy range of ± 0.5° C.

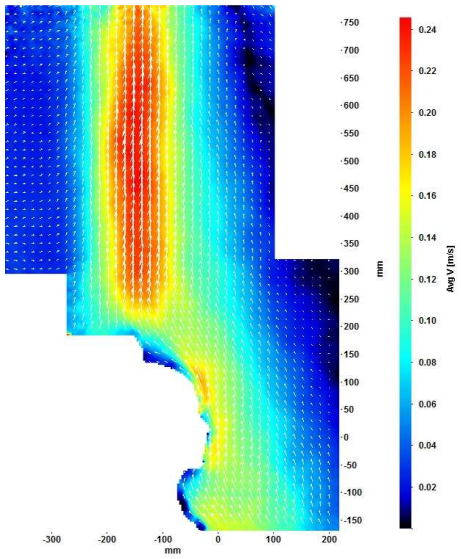

Figure 11 Average velocity contours (over 10 minutes) obtained using PIV in the chamber.

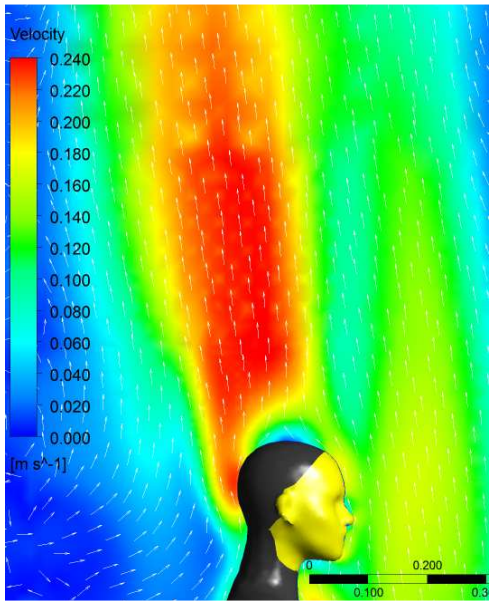

Figure 12 Average velocity contours obtained using steady state CFD simulations with RNG-k-ε model.

Both SST and RNG-k-ε model show 6% and 8% difference from the temperature values near the inlet. For the rest of the sensor points, RNG-k-ε model predicts percentage differences less 2.6%. SST Turbulence model seem to over-estimate the temperature field.

PIV results shown in Figure 10 illustrate the zones of high turbulence associated with Buoyancy driven flows. The instantaneous velocities once averaged using LaVision DaVis PIV processing software show a stable and well developed thermal plume as shown in Figure 11 which are well comparable with the steady state CFD simulation results shown in Figure 12 and Figure 13.

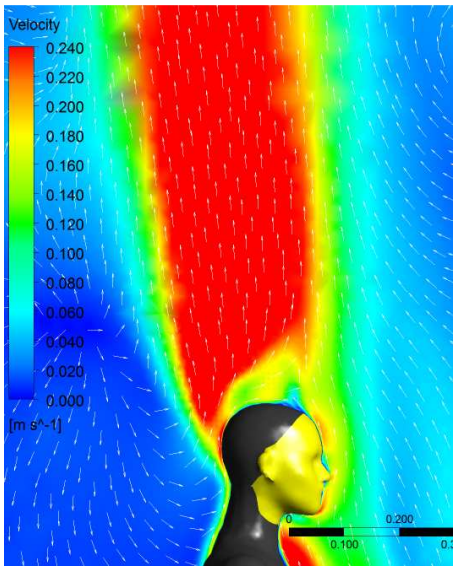

Figure 13 Average velocity contours obtained using steady state CFD simulations with SST model.

The difference in the two simulation models lie in the numerical implementation of the model and need to be investigated separately. In general the simulation results presented in Figure 12 using RNG k-ε turbulence model depict closely the results obtained using PIV tests. Simulation results based on SST turbulence model show a wider thermal plume with higher velocities as compared to measurements and RNG-k-ε model. The maximum average velocity in the thermal plume obtained using PIV is 0.26 m/s where as the maximum average velocity in the thermal plume using CFD simulations are 0.25 m/s and 0.38 m/s for RNG- k-ε and SST Turbulence models respectively. The maximum y+ values on the surface of Victoria for simulation with SST Turbulence model was found to be 3.6 whereas for RNG-k-ε a y+ value of 1.7 was found. In order to have a lower y+ value using SST Turbulence model, a finer mesh near to the surface of Victoria need to be generated. Using a different mesh would lead to a mesh inconsistency thereby not allowing the comparison of results between the two simulations.

CONCLUSIONS

Simulation results based on the SST turbulence model show a wider thermal plume with higher velocities compared to measurements and the RNG k-ε model. Similar behaviour was also observed by Cook et al. (1998) when using the standard k-e model where a wider plume was thought to be caused by over-prediction of entrainment into the plume. As the SST model blends a k-ω model in the near wall region with a k-ε model in the outer region, it is likely that the SST model exhibits similar characteristics in terms of plume entrainment. In addition, it is possible that the SST model in the current work is over-predicting the heat transfer coefficient at the body surface thus leading to a higher temperature around the body compared to the RNG model. This would lead to greater buoyancy forces and higher velocities. This postulation needs to be investigated further.

On the basis of the presented study, it can be concluded that RNG- k-ε model closely predict (with less than 3% difference in the thermal plume region) the flow fields associated with the thermally induced flows generated due to human metabolic heat. In literature SST turbulence model is mentioned to be more suitable for flows dominated by wake and shear regions e.g. by Yang (Yang, 2007). In order to exploit the full potential of the SST model reported by the code developer (Ansys Inc. 2011) for buoyancy driven flows, more investigation need to be carried out with major focus on meshing and numerical modelling requirements such as y+.

In the present study PIV has been successfully employed for investigating flow fields induced due to low buoyancy driven forces. PIV however has its limitations when applying for cases involving complex geometrical configurations e.g. limitation in FoVs, sensitivity in terms of placement and control of devices etc.

Due to the expensive equipment, time constraints and limited FoV, PIV is more suited to detailed investigation of flow fields over a small area. PIV results can be used to validate full scale CFD models. The information and knowledge gained by PIV and validated CFD models can then be applied for large scale and complex environments with a higher level of confidence in results.

FUTURE WORK

In light of the presented study, recommendations for future work are made. These recommendations for future work are listed below.

- Investigation of entrainment and heat transfer effects as predicted by RNG-k-ε and more advance SST turbulence models.
- Combination of PIV and CFD for investigation of entrainment effects.
- Use of validated CFD model for contamination transport in indoor climates for single and multiple occupancy.
- Entrainment and transport of CO2 in the thermal plume

REFERENCES

Ansys Inc. 2010. Ansys CFX 12.1 user manual.

Ansys Inc. 2010. Ansys ICEM CFD 12.1 user manual.

Borges.C.P, Quintela.D.A, Brites.G.N, Gasper.A.R, Costa.J.J (2002), Analysis of thermal plumes generated by a seated person, a thermal manikin and a dummy, in: Proceedings of the 8th International Conference on Air Distribution in Rooms – Roomvent 2002, Copenhagen, vol. 1, 2002, pp. 253–256.

Clark.R.P and Toy.N (1975), Natural convection around the human head, J. Physiol. 1975 January; 244(2): 283–293.

Cook, M.J. and Lomas, K.J., "Buoyancy Driven Displacement Ventilation Flows : Evaluation of Two Eddy Viscosity Turbulence Models for Prediction", Building Services Engineering Research and Technology, 19(1), 1998, 15-21, ISSN : 0143-6244.

Cropper.P.C, Yang.T, Cook.M.J, Fiala.D, Yousaf.R, 2008."Exchange of simulation data between CFD programmes and a multisegmented human thermal comfort model". Proceedings of the 5th Windsor Conference, Air Conditioning and the Low Carbon Cooling Challenge, Cumberland Lodge, Windsor, UK, 27-29th July 2008. London: Network for Comfort and Energy Use in Buildings, http://nceub.org.uk.

Hayashi.T, Yoshiaki.I, Shinsuke.K, Murakami.S, (2002). "CFD analysis on characteristics of contaminated indoor air ventilation and its application in the evaluation of the effects of contaminant inhalation by a human occupant", Building and Environment, Volume 37, 2002 , pp. 219-230.

Homma, H. (1988) Examination of free convection around occupant′s body caused by its metabolic heat, ASHRAE Transactions 94(1): pp 104-124

LaVision,GmbH,Website:http://www.lavision.de/ en/techniques/piv.php

Melikov A, Zou H, (1999), "Comparison of methods for determining equivalent temperature under well-designed conditions". Proceedings of the Sixth International Conference FLORENCE ATA, Firenze, Italy, 1999.

Melikov A, Cermak R, Mayer M. (2002), "Personalized ventilation: Evaluation of different air terminal devices". Energy and Buildings 2002; 34 (8):829-36

Murakami.S, Kato.S Zeng.Jie, (2000), "Combined simulation of airflow, radiation and moisture transport for heat release from a human body", Building and Environment, Volume 35, 2000 , pp. 489-500

Nielsen P.V, Murakami.S, Kato. S, Topp.C and Yang.J, "Benchmark tests for a computer simulated person".from: http://www.civil.auc.dk.

Özcan, O., Meyer, K.E. and Melikov, A. (2005), “A Visual Description of the Convective Flow Field around the Head of a Human”, Journal of Visualization, 8, 23-31, 2005.

Rhinoceros 3.0, NURBS Modelling for windows, McNeel Europe.

Sideroff, C.N. and Dang, T.Q. (2005). "Validation of CFD for the flow around a computer simulated person in a mixing ventilated room," Proceedings of the 10th International Conference on Indoor Air Quality and Climate, Beijing, China, 3885-3889.

Siegel.R, Howel. J.R., "Thermal Radiation Heat Transfer", (1992), 3rd Edition, Hemisphere Publishing.

Sørensen D.N., Vøigt L.K. (2003), "Modelling flow and heat transfer around a seated human body by computational fluid dynamics". Building and Environment, Volume 38, June 2003 , pp. 753-762.

Spitzera.I.M, David R. Marrb, , and Mark N. Glausera (2010), Impact of manikin motion on particle transport in the breathing zone. Journal of Aerosol Science, Volume 41, Issue 4, April 2010, pp 373-383.

Tanabe S, Arens EA ,Bauman FS, Zhang H, Madsent T.L, (1994), "Evaluating thermal environments by using a thermal manikin with controlled skin surface temperature". ASHRAE Transactions 1994; 100(1): 39-48

Topp.C, (2002). "Influence of geometry of a computer simulated person on contaminant distribution and personal exposure". Proceedings of ROOMVENT 2002, Eighth International Conference on Air Distribution in Rooms, Copenhagen, Denmark.

Yang.T, Cropper.P.C, Cook.M.J, Yousaf.R and Fiala.D, (2007). "A new simulation system to predict human-environment thermal interactions in naturally ventilated buildings". Proceedings of the 10th International Conference on Building Simulation (Building Simulation 2007), Tsinghua University, Beijing, China, 3rd-6th September, Paper ID-424, pp. 751-756

Yousaf.R, Using CFD for predicting heat and mass transfer phenomena associated with human thermal comfort and indoor air climate, PhD research Interim report, Loughborough University, August 2010.